

The evolution of actively star forming galaxies in the mid infrared.

O. Vega¹, L. Silva², P. Panuzzo³, A. Bressan³, G. L. Granato³, & M. Chavez¹

¹INAOE, Luis Enrique Erro 1, 72840, Tonantzintla, Puebla, Mexico

²INAF-Trieste, Via Tiepolo 11, I-34131 Trieste, Italy

³INAF-Padova, Vicolo dell'Osservatorio 5, I-35122 Padova, Italy

Accepted. Received

ABSTRACT

In this paper we analyze the evolution of actively star forming galaxies in the mid-infrared (MIR). This spectral region, characterized by continuum emission by hot dust and by the presence of strong emission features generally ascribed to polycyclic aromatic hydrocarbon (PAH) molecules, is the most strongly affected by the heating processes associated with star formation and/or active galactic nuclei (AGN). Following the detailed observational characterization of galaxies in the MIR by ISO, we have updated the modelling of this spectral region in our spectro-photometric model GRASIL (Silva et al. 1998). In the diffuse component we have updated the treatment of PAHs according to the model by Li & Draine (2001). As for the dense phase of the ISM associated with the star forming regions, the molecular clouds, we strongly decrease the abundance of PAHs as compared to that in the cirrus, basing on the observational evidences of the lack or weakness of PAH bands close to the newly formed stars, possibly due to the destruction of the molecules in strong UV fields. The robustness of the model is checked by fitting near infrared to radio broad band spectra and the corresponding detailed MIR spectra of a large sample of galaxies (Lu et al. 2003), at once. With this model, we have analyzed the larger sample of actively star forming galaxies by Dale et al. (2000). We show that the observed trends of galaxies in the ISO-IRAS-Radio color-color plots can be interpreted in terms of different evolutionary phases of star formation activity, and the consequent different dominance in the spectral energy distribution (SED) of the diffuse or dense phase of the ISM. We find that the observed colors indicate a surprising homogeneity of the starburst phenomenon, allowing only a limited variation of the most important physical parameters, such as the optical depth of the molecular clouds, the escape timescale of young stars from their formation sites, and the gas consumption timescale. In this paper we do not attempt to reproduce the far infrared (FIR) coolest region in the color-color plots, since we concentrate on models meant to reproduce active star forming galaxies, but we discuss possible requirements of a more complex modelling for the coldest objects.

Key words: galaxies: evolution – galaxies: ISM – galaxies: starburst – infrared: galaxies – ISM: dust, extinction, PAHs

1 INTRODUCTION

With the advent of the new generation of infrared space telescopes it has become possible to study in great detail the mid-infrared (MIR) spectral region of galaxies, that had been previously sampled only with broadband filters by IRAS. Besides the hot continuum emission, an important component observed in the MIR spectra of many dusty galactic and extragalactic objects is constituted by strong emission features at 3.3, 6.2, 7.7, 8.6, 11.3 and 12.7 μm . These features are most commonly ascribed to aromatic C-

C and C-H vibrations in large planar Polycyclic Aromatic Hydrocarbons (PAH) molecules, with size $\sim 10 \text{ \AA}$ and containing $\sim 50 - 100$ C atoms (Leger & Puget 1984; Allamandola et al. 1985; Puget & Leger 1989; Tielens et al. 1999).

The environmental conditions that may contribute to the MIR continuum emission are quite well understood in terms of a strong radiation field that heats dust at the required temperatures. Such regions are mainly located in the vicinity of hot stars, in the AGN torii and in dense circumstellar envelopes of cool evolved stars. Conversely our knowledge of the origin of PAH emission is still controver-

sial, in spite of its importance for an accurate modelling of the MIR spectral region.

Detailed observations with ISO have allowed deep investigations of the properties and variations of PAH features in different Galactic environments - post-AGB stars, planetary nebulae, reflection nebulae, young stellar objects, HII regions and photo-dissociation regions (PDR), diffuse interstellar medium -, as well as in different galaxies (e.g. Cesarsky et al. 1996; Verstraete et al. 1996; Beintema et al. 1996; Boulanger et al. 1996; Mattila et al. 1996; Peeters, Spoon, & Tielens 2004a; see the review by Peeters et al. 2004b and references therein). The aromatic emission features in most galaxies have been found to be very similar to those in Galactic star forming regions and in the cirrus (Metcalfe et al. 1996; Vigroux et al. 1996; Genzel et al. 1998; Lutz et al. 1998; Rigopoulou et al. 1999; Tielens 1999; Helou et al. 2000; Forster Schreiber et al. 2003; Lu et al. 2003). However MIR spectra with different appearances have been observed in peculiar environments, with particularly strong radiation fields (e.g. in AGNs, Genzel et al. 1998; Lutz et al. 1998). This has led to the use of PAH emission as a tracer of the star formation process (Roussel et al. 2001, Forster Schreiber et al. 2004), and its lack as indicative of an AGN dominated emission mechanism (Genzel et al. 1998; Clavel et al. 2000; Laurent et al. 2000).

More recently, a comprehensive analysis of the MIR to FIR spectra of Galactic star forming regions, normal galaxies and starbursts suggests that PAHs are a better tracer of B stars rather than of massive O stars (Peeters et al. 2004a, Boselli, Lequeux, & Gavazzi 2004, Madden 2005). This has been found also by Tacconi-Garman et al. (2005) by direct high resolution $3 \mu\text{m}$ imaging of two nearby starbursts (NGC253 and NGC1808): they find no spatial coincidence between the detailed distribution of PAH emission and the sites of the most recent star formation.

Several recent works have also shown that the intensity of the PAH bands is systematically lower in very low metallicity galaxies, such as Blue Compact Dwarfs and dwarf galaxies in general, and some irregulars (e.g. Madden 2000; Galliano et al. 2003, 2005; Boselli et al. 2004; Dale et al. 2005; Engelbracht et al. 2005). This has been ascribed either to a lower intrinsic PAH abundance or to a higher destruction rate of these molecules due to a strong UV field (see e.g. the review by Madden 2005).

In summary there is mounting evidence that the use of the MIR region and in particular of the PAH features as tracers of star formation in galaxies is not straightforward.

In order to correctly interpret the spectra of galaxies, a detailed modelling that includes the complex interaction between the evolution of stellar populations and dust is needed. In fact while the new observations have allowed us to better define the characterization of PAHs in the diffuse medium (e.g. Li & Draine 2001; Zubko, Dwek, & Arendt 2004), most current spectro-photometric models adopt a pure phenomenological approach (e.g. Dale et al. 2001). A recent model that combines radiation transfer within the star forming regions with the evolution of the powering star clusters is presented by Dopita et al. (2005). This model, though being the most advanced in the specific treatment of the star forming regions, lacks the diffuse component and cannot be safely compared with galaxies as a whole. On the

other hand the PAH treatment in our code GRASIL¹ (Silva et al. 1998), that takes into account the entire temporal evolution of several subcomponents, was still based on pre-ISO data.

For this reason we present here an updated version of GRASIL including the new developments for the PAH emission, and perform an analysis of the evolution of *normal metallicity* (i.e. not dwarf galaxies whose MIR SEDs are observed to behave differently as recalled above) actively star forming galaxies in the mid infrared.

The structure of the paper is the following. In Section 2 we summarize the inclusion of the new theoretical model of PAHs by Li & Draine (2001, LD01 hereafter). There we make the important assumption, supported by observations, that the PAH abundance within our (star-forming) molecular clouds (MC) is significantly depleted with respect to that in the cirrus component. In Section 3 we perform a detailed comparison of the new model with NIR to radio SEDs of star forming galaxies taken from the Lu et al. (2003) sample. We show that, together with the wide NIR-Radio broad band fluxes, also the MIR-ISO narrow bands, dominated by PAH emission, are very well reproduced. Since these galaxies span a wide range of FIR luminosities, we conclude that a proper combination of a cirrus component with PAH emission suited for the diffuse ISM in our Galaxy (where the LD01 model is calibrated), and a MC component with strongly depleted PAHs, can be safely adopted in general for star forming galaxies. With this new model we explore the MIR-FIR-radio colors of a larger sample of galaxies taken from Dale et al. (2000) for which only broadband ISO, IRAS and Radio fluxes are available (Section 4). This comparison allows us to draw a physical interpretation of the observed data, in terms of the evolution of the starburst phenomenon. The MID-FIR and Radio data constitute a unique set of constraints indicating a strong homogeneity of the main physical parameters. Our conclusions are summarized in Section 5.

2 PAH MODELLING IN GRASIL

In this Section we provide a short summary of the properties of GRASIL. We defer the reader to Silva et al. (1998) and Silva (1999) for further details.

GRASIL calculates the UV to radio SED of galaxies by taking into account a detailed treatment of dust reprocessing of stellar radiation. A particular important point is that the coupling between stars and dust is considered, by letting stars form inside optically thick molecular clouds (MCs) and then gradually escape as they grow old. Older stellar generations are distributed within the diffuse ISM (cirrus). This modelling, with a realistic 3-D treatment of extinction and IR emission, allows quantitative physical interpretations of multi-wavelength observations as well as predictions (e.g. Silva et al. 1998; Granato et al. 2000; Panuzzo et al. 2003, 2004).

In addition to the complex geometry, the SEDs depend on the dust intrinsic properties (chemical composition, size

¹ Available at <http://adlbitum.oat.ts.astro.it/silva/default.html> or <http://webpd.astro.it/granato/grasil.html>

distribution, shape, see the recent reviews by Draine 2003 and Dwek 2004). These properties depend on the different environments in which dust grains form or evolve. Most of the available dust models are suited for the Galactic cirrus, for which the largest data set is available. The dust model we use in GRASIL is made of graphite and silicate spherical dust grains (Draine & Lee 1984 and Laor & Draine 1993), with a power-law size distribution that extends to include also the very small grains transiently heated by single photons, and by PAH molecules. The dust heating and emission are adequately computed for each component.

2.1 PAH emission in the cirrus component

In Silva et al. (1998) we took into account five PAH emission bands, at 3.3, 6.2, 7.7, 8.6 and 11.3 μm . We adopted the optical-UV absorption cross-section by Leger, D’Hendecourt & Defourneau (1989), obtained by laboratory measurements for different PAH mixtures. We followed Leger et al. (1989) for the heat capacity as a function of temperature and number of C and H atoms in the molecules. We adopted a population of PAHs with a continuous power-law distribution, $dn/dN_C \propto N_C^{-2.25}$, with N_C , the number of Carbon atoms in the molecules, extending from 20 to 280 atoms. This range corresponds to a size $a = 4$ to 15 \AA , with $a = 0.9\sqrt{N_C}$ (valid for the catacondensed PAHs, the most compact and stable configuration). We took into account the possibility of partial hydrogenation of the molecules, as suggested by observations, and fixed the hydro-coverage (the ratio of the number of H atoms over the number of available sites) so to reproduce the observed ratio of C-H and C-C bands in the Galactic cirrus. The abundance of carbon atoms locked in PAHs in our dust model is set to 18 ppm in the cirrus, and was 10 times lower in the MCs to account for PAH destruction in strong UV fields (see Section 2.2).

The PAH emissivity is computed following mainly Xu & De Zotti (1989). Once emitted, PAH bands are absorbed by MCs and/or cirrus dust before emerging from the model galaxy. This treatment provides a rigorous computation of the total energy emitted in these features.

ISO data have allowed us to get a deeper knowledge of PAH phenomenology, as summarized in the Introduction. In particular, new PAH bands have been detected, their profiles studied in different environments and galaxies, thus yielding several constraints for their modelling. Nevertheless, the properties of astrophysical PAHs are still rather uncertain, so that, as in the case of dust models in general, their modelling still require ad-hoc settings of parameters to best reproduce the observations.

Li & Draine (2001) presented a quantitative model for dust in the diffuse ISM, including PAHs. Basing on laboratory studies of these molecules, and by comparing with observations, they have provided “astronomical” cross sections for PAHs, reproduced with Drude profiles. We have updated our model for PAHs in GRASIL by adopting the main features of the LD01 model: in addition to the 3.3, 6.2, 7.7, 8.6, 11.3 μm bands, we now include also the 11.9, 12.7, 16.4, 18.3, 21.2, and 23.1 μm bands. Absorption and emission from PAHs are computed as described above, but adopting the FWHM and emission cross sections by LD01. As stressed by the authors, available laboratory data on PAHs differ by large factors among different groups, and also between ex-

Table 1. Properties of the Lu et al. (2003) sub-sample. The galaxies are ordered by increasing $\log(f_\nu(60\mu\text{m})/f_\nu(100\mu\text{m}))$. Column (3) displays the fraction of the LW2 flux from the cirrus component over the total LW2 flux of the best fit model. Column (4) shows the main contributor to the MIR SED of the best fit, “c” indicates that the MIR SED is “cirrus emission dominated”, “m” indicates that it is “molecular cloud emission dominated”, and “mix” that the MIR SED is a mixed of these two contributions, see Fig. 2. We classify the fit as “c” if the ratio $F_{\text{LW2(cirrus)}}/F_{\text{LW2(total)}}$ is $\geq 2/3$, as “mix” if $1/3 \leq F_{\text{LW2(cirrus)}}/F_{\text{LW2(total)}} < 2/3$ and as “m” if $F_{\text{LW2(cirrus)}}/F_{\text{LW2(total)}} < 1/3$.

Galaxy	$\log\left(\frac{f_\nu(60\mu\text{m})}{f_\nu(100\mu\text{m})}\right)$	$\frac{F_{\text{LW2(cirrus)}}}{F_{\text{LW2(total)}}$	PAHs fit
NGC6286	-0.44	0.851	c
NGC3583	-0.42	0.744	c
IC3908	-0.33	0.768	c
UGC2238	-0.30	0.785	c
NGC7771	-0.30	0.694	c
NGC5713	-0.24	0.543	mix
NGC2388	-0.17	0.461	mix
NGC4102	-0.16	0.460	mix
NGC3885	-0.15	0.541	mix
NGC1482	-0.14	0.471	mix
NGC4691	-0.14	0.384	mix
NGC1022	-0.13	0.253	m
NGC1222	-0.07	0.211	m
NGC4194	-0.01	0.062	m

perimental results and theoretical calculations. Therefore, LD01 modified laboratory data for the emission cross sections in order to reproduce observations (the Galactic cirrus emission).

The LD01 model for PAHs above 14 μm is based on laboratory data from Moutou et al. (1996), since galaxy spectroscopy was not available. Very recently, some works have reported Spitzer spectra that probe this poorly known region (e.g. Armus et al. 2004; Peeters et al. 2004c; Smith et al. 2004; Weedman et al. 2005). In some cases, several new PAH features have been observed between ~ 17 and 22 μm , but not coincident with the 18.3, 21.2, and 23.1 μm bands of the model. Instead, in Smith et al. (2004), no PAH band has been observed above $\sim 18\mu\text{m}$ in NGC 7331. Note anyway that these uncertainties are not expected to affect our results. Indeed we have estimated the contribution of the 18.3, 21.2, and 23.1 μm bands to the 25 μm IRAS filter as compared to the continuum, for the models fitting the SEDs described in Section 3. This estimate refers to the worst case, in which no PAH features are present in galaxies above $\sim 18\mu\text{m}$. In most cases the contribution is less than 10%, only in a couple of cases it is $\lesssim 30\%$, i.e. we are always within the IRAS observational errors. We also note that the LD01 model fits very well the DIRBE data for dust emission in our Galaxy (figures 8 and 10 in LD01), with one of the DIRBE filters dominated by these three bands. It is conceivable that in a few years it will become possible to have enough observational constraints to better define a reference model for astrophysical PAHs at long wavelengths.

2.2 PAH emission in the MC component

While the abundance of PAHs in the cirrus environment is relatively constrained, the situation is much less clear for the regions of intense star formation, characterized by higher particle densities and/or larger UV radiation fields. Abergel et al. (1994) already noticed a lack of PAH emission in dense molecular clouds revealed by ^{13}CO . Marty et al. (1994) advanced a possible explanation suggesting that in these clouds PAH molecules could be depleted by accretion onto dust grains and/or formation of organometallic complexes (see also Serra et al. 1992). Concerning the effects of strong UV radiation field, Allain, Leach, & Sedlmayr (1996) showed that PAH molecules which are already either ionized or even partially dehydrogenated, have photo-dissociation rates far in excess of those of the neutral species.

Only after ISO data were available, it was possible to build a clearer and more direct picture of PAH emission, revealing a general lack of such features in regions associated with the star formation processes. Observations in our Galaxy show a clear decreasing of PAH emission near hot stars, or when passing inward from PDRs to HII regions (Boulanger et al. 2000; Contursi et al. 2000). Hony et al. (2001) report observations of a high degree of dehydrogenation in star forming regions. Peeters, Spoon, & Tielens (2004a) show a lack of the PAH features in spectra of ultra compact HII regions, and in that of heavily obscured starbursts, both characterized by high dust optical depths. These latter observations are particularly relevant because they raise the question whether such a lack is due to a strong attenuation accompanied by dilution of the continuum, or to a real destruction of PAH molecules in such environments. To clarify this point we performed several tests with models of molecular clouds with GRASIL, varying the optical depth, the abundance of PAHs and the sublimation temperature of the dust (the latter in order to allow dilution by hot dust). It resulted that the only viable way to suppress PAH emission in our MC models was to deplete their abundance by a large factor ($\simeq 1000$ with respect to that of the cirrus in order to reproduce the MIR observations described below). Thus we will assume in the following that the abundance of PAHs in our MCs is fixed to 10^{-3} times that in the cirrus. This is even more evident if one thinks that the lack of the $3.3 \mu\text{m}$ PAH emission near very hot stars observed by Tacconi-Garman et al. (2005) is difficult to ascribe to dilution by the continuum.

The necessity of such a strong damping has been considered also by Dale et al. (2001). In their phenomenological IR SEDs, they adopted an analytical damping factor for PAHs, function of the intensity of the radiation field. From their treatment one sees that when the radiation intensity is larger than a few thousands time the local interstellar radiation field, the PAHs are almost completely depleted.

Finally let us comment that observations indicate that PAH emission in star forming environments arise mainly from PDR regions. These regions are implicitly accounted for in our treatment, because it accounts for absorption of dissociating photons in the interior of the molecular clouds and in the surrounding diffuse medium. In principle our code allows us to consider a distribution of MCs with different optical depths (Silva 1999), in particular we could include a class of low optical depth molecular clouds where PAHs are

not depleted. While this would allow us to explicitly model the PDR regions (and will be the subject of a forthcoming paper), this would introduce another set of free parameters that appear not to be relevant for the actively star forming galaxies we compare with below, as illustrated in the following sections.

3 COMPARISON WITH MID INFRARED SEDS OF SELECTED GALAXIES

In order to test the model with observations we performed a detailed comparison with well observed MIR SEDs of a sample of star forming galaxies taken from Lu et al. (2003). This galaxy sample, observed with the PHT-S mode of ISOPHOT ($5.8 - 11.6 \mu\text{m}$), covers the full range of morphological types of disk galaxies, from S0 to Im, and is characterized by an increasing ratio of present day star forming activity to the past time averaged star formation rate (Helou 1986). The Lu et al. galaxies are a subset of a larger sample for which ISO (Dale et al. 2000) and IRAS broad band fluxes are available, and will be discussed in Section 4.

Among this sample, we selected those galaxies which are classified as HII on the NED², and with well defined PAH features, i.e. we considered those objects whose data are incompatible with an absence of features when including error bars. The selected sub-sample is listed in Table 1, where galaxies are reported in increasing order $f_{\nu}(60\mu\text{m})/f_{\nu}(100\mu\text{m})$ together with one of the results of the fitting, i.e. if the galaxy is found to be cirrus dominated (c type in the last column), molecular cloud dominated (m) or of mixed type respectively. The other properties of these galaxies can be retrieved in Table 4.

Lu et al. provide specific fluxes within narrow square passbands around the corresponding PAH features, for an aperture of $24'' \times 24''$. In order to compare these values with the global broad-band photometry at $6.75 \mu\text{m}$ (LW2) taken by Dale et al. (2000), we used the aperture coverage factor, p , given by Lu et al. With this factor, the errors in the fit of the PAH bands by using the $6.75 \mu\text{m}$ broadband is always less than 25%.

The fits of the observed SEDs were performed on a wider wavelength range (from NIR to radio, using H, J, K bands, LW2, LW3 ISO bands, 12, 25, 60 and $100 \mu\text{m}$ IRAS bands, 450, 850 μm SCUBA bands, and 8.4, 4.8, and 1.49 GHz bands when the data are available, see below and Fig. 1) and by taking into account the suitable filter responses.

We considered galaxy models spanning a wide range of parameters: star formation history, obscuration times, dust optical properties, etc. The star formation history was obtained with our chemical evolution code, adopting a Schmidt-type SFR ($= \nu_{\text{SCh}} M_{\text{gas}}$), with a star formation efficiency $\nu_{\text{SCh}} = 0.5 \text{ Gyr}^{-1}$, a Salpeter (1955) IMF ($\propto M^{-1.35}$) between $0.05 - 120 M_{\odot}$. The observational sample is made of star forming galaxies with a large range of IR luminosities,

² The NASA/IPAC Extragalactic Database is operated by the Jet Propulsion Laboratory, California Institute of Technology, under contract with the National Aeronautics and Space Administration.

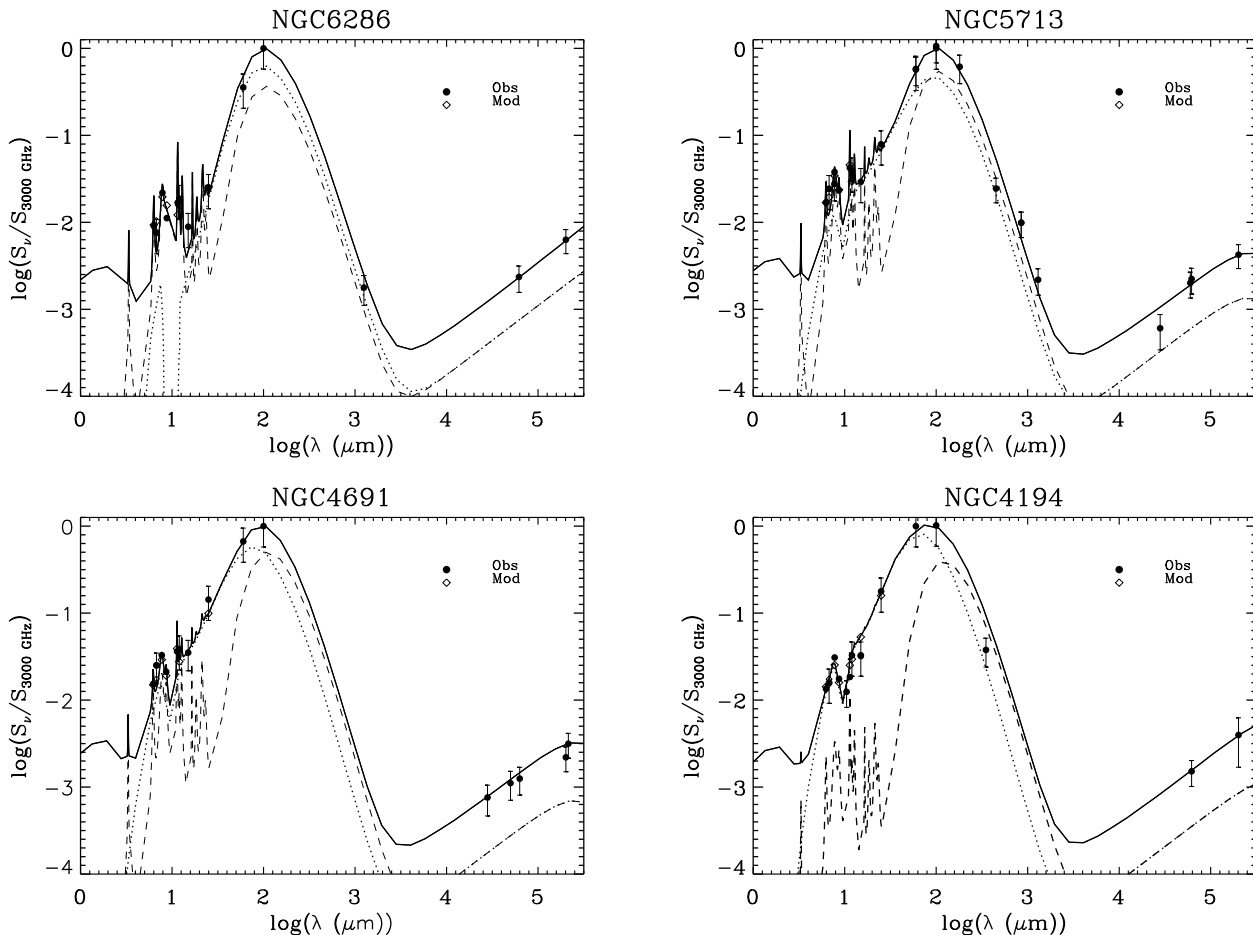


Figure 1. Comparison between the observed and model SEDs for four representative galaxies of our sample. The solid line is the total emission, the dashed line is the contribution from the diffuse medium, and the dotted line is the contribution from the molecular clouds. Filled circles are the observational data by Lu et al. (2003), Bendo et al. (2002), Dale et al. (2000), Dunne et al. (2000), Machalski & Condon (1999), Chini et al. (1996, 1995), Condon et al. (1995, 1990), Niklas et al. (1995), Carico et al. (1992), and Israel et al. (1983). Open rombs are for the model in the following order: 6.2 μm , 6.75 μm (ISO LW2), 7.7 μm , 8.6 μm , 11.3 μm , 12 μm (IRAS), 15 μm (ISO LW3) and 25 μm (IRAS).

revealing the presence of mild to strong starbursts. Therefore we superimposed to the quiescent component a starburst phase characterized by an exponential decreasing star formation rate (with e-folding times t_b). The burst is supposed to start at a galaxy age of 11.95 Gyr, and to involve 10% of the mass of the gas present at that age. We follow the evolution of the SEDs at different ages of the superimposed burst (age_b), from the early starburst phase to the post-starburst and quiescent-normal phase.

Among the GRASIL parameters that mostly affect the MIR-FIR range we recall the optical depth of MCs (we address to it as τ_1 , i.e. at 1 μm), the gas-to-dust mass ratio (G/D), the fraction of molecular mass to total gas mass (M_m/M_{gas}), and the escape time-scale of newly born stars from their parent MCs (t_{esc}). Tables 2 and 3 list the ranges of parameters of the model SED library used to perform the fits.

In Fig. 1 we show some examples of the full SED fittings we performed to the galaxy sample of Table 1. The galaxies shown in the figure are representative of the range of $f_\nu(60\mu\text{m})/f_\nu(100\mu\text{m})$ values covered by the sample.

Table 2. Parameters for the star formation history of the model library. M_{low} and M_{up} are the adopted mass limits of the Salpeter IMF; ν_{Sch} is the efficiency of the Schmidt-type SFR; t_b indicates the e-folding time of the exponential burst superimposed to the quiescent star formation; age_b indicates the ages, from the beginning of the burst, at which the SEDs are computed; $\%M_b$ is the percentage of the mass of gas of the galaxy models involved in the burst at an age of 11.95 Gyr. See text for more details.

M_{low} M_\odot	M_{up} M_\odot	ν_{Sch} (Gyr^{-1})	t_b (Myr)	$\log(age_b)$ (yr)	$\% M_b$
0.05	120	0.5	10 - 50	6.0 - 8.2	10

In Fig. 2 we show the detailed comparison in the MIR range between our best fitting models and the data for all the galaxies reported in Table 1. The points in the figure refer to the specific fluxes at 6.2 μm , 6.75 μm (ISO LW2), 7.7 μm , 8.6 μm , 11.3 μm , 12 μm (IRAS), 15 μm (ISO LW3) and 25 μm (IRAS). In all cases the predicted PAH features compare very well with the observations being generally within

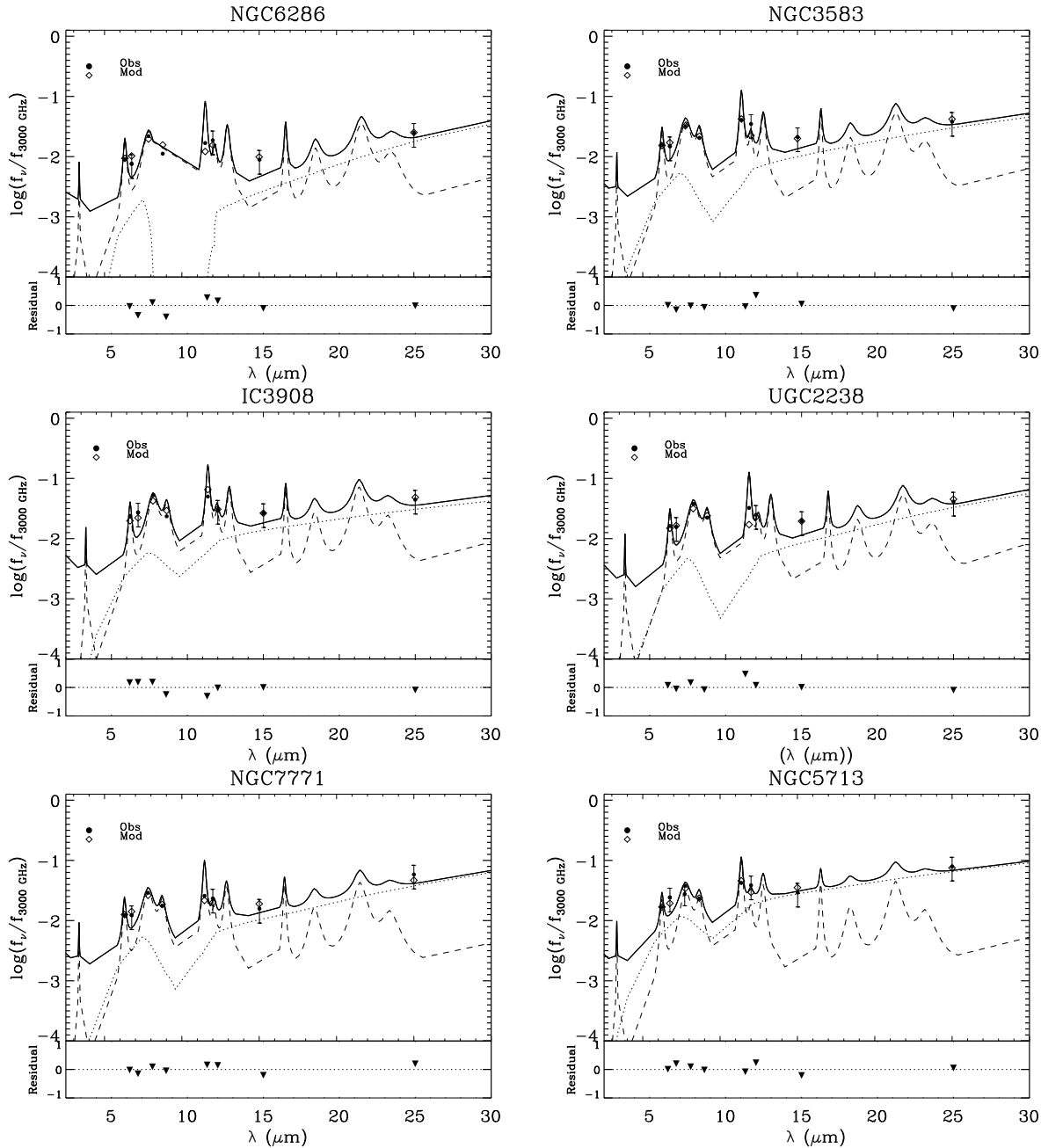


Figure 2. Detailed comparison between the observed and model PAH bands. The solid line is the total emission, the dashed line is the contribution from the diffuse medium, and the dotted line is the contribution from the molecular clouds. Filled circles are the observational data by Lu et al. (2003) and Dale et al. (2000), in the following order: $6.2\mu\text{m}$, $6.75\mu\text{m}$ (ISO LW2), $7.7\mu\text{m}$, $8.6\mu\text{m}$, $11.3\mu\text{m}$, $12\mu\text{m}$ (IRAS), $15\mu\text{m}$ (ISO LW3) and $25\mu\text{m}$ (IRAS). Open rombs are for the model. The residuals between models and data are given as $(f_{\text{data}} - f_{\text{model}})/f_{\text{data}}$. In all cases the MIR continuum is mostly dominated by the molecular clouds emission, while the bands containing PAHs are initially dominated by the cirrus component, and then by the molecular contribution, at increasing $f_{\nu}(60\mu\text{m})/f_{\nu}(100\mu\text{m})$ flux ratio.

the quoted standard deviations. We also notice, from Table 1 that, at increasing $f_{\nu}(60\mu\text{m})/f_{\nu}(100\mu\text{m})$ ratio, the SEDs shift from cirrus dominated to MC dominated, without any appreciable trend in the goodness of the fit. Given the wide range of the luminosity ratios $L_{\text{FIR}}/L_{\text{B}}$ spanned by the sample galaxies, we conclude that the model is robust and able to reproduce the continuum SEDs as well as the MIR spec-

tral features, over a wide range of relative star formation activity, from mild to strong starbursts.

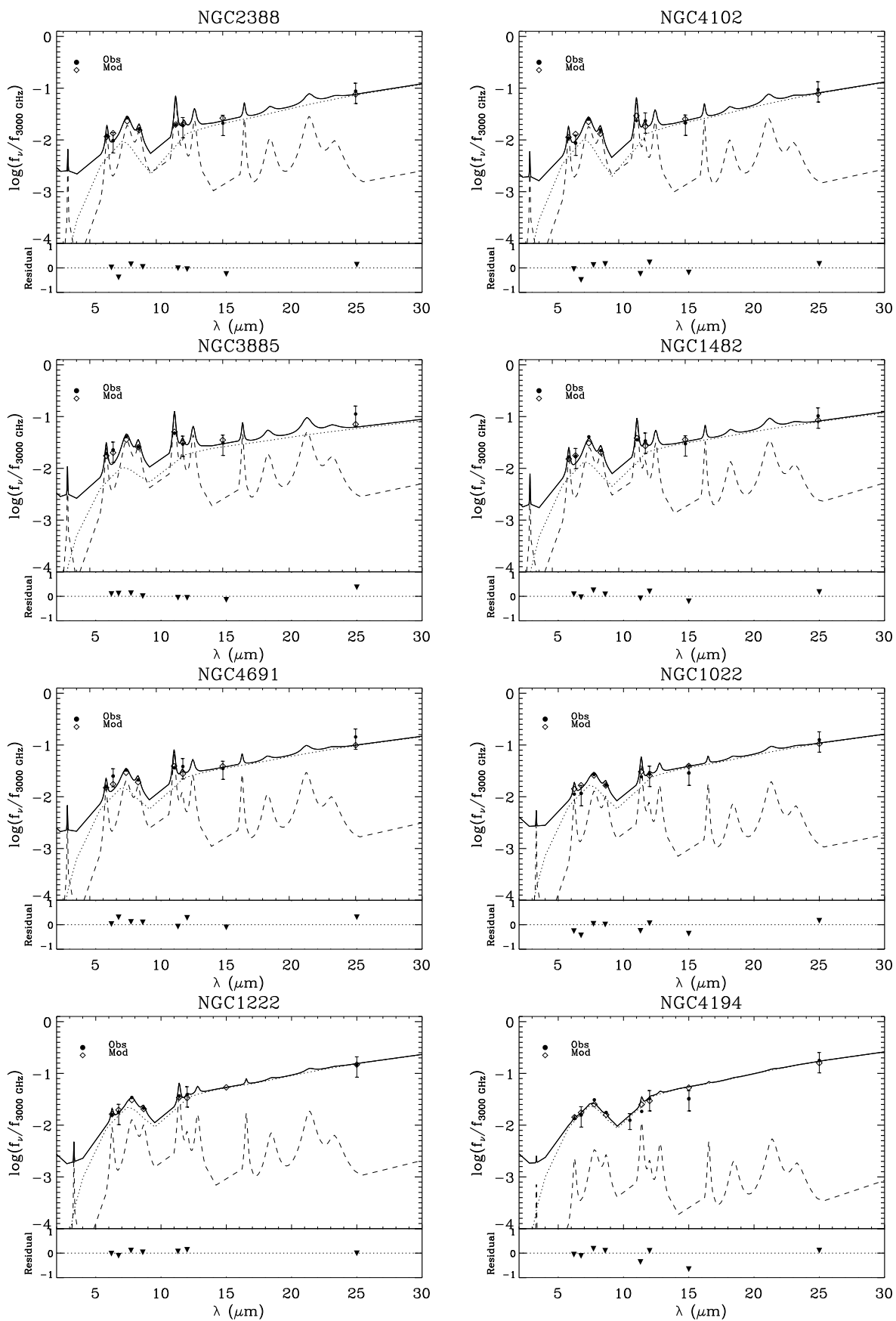


Figure 2. Continued

Table 3. GRASIL parameters for the SED model library. G/D is the gas to dust mass ratio; t_{esc} is the escape time scale of newly born stars from their parent MCs; $\frac{M_m}{M_{\text{tot}}}$ is the fraction of gas in MCs; τ_1 is the $1\mu\text{m}$ optical depth of MCs

G/D	t_{esc} (Myr)	$\frac{M_m}{M_{\text{tot}}}$	τ_1
100	10 - 50	0.1 - 0.9	4 - 180

4 COMPARISON WITH ISO-IRAS COLOR-COLOR PLOTS

We now compare our models with a larger data set of star-forming galaxies for which only broad-band ISO and IRAS fluxes are available.

4.1 The data sample

This observational sample is taken from Dale et al. (2000). They published global ISO fluxes for a large sample of galaxies, for which also IRAS data are available. These galaxies were observed within the ISO Key Project on the Interstellar Medium of Normal Galaxies (Helou et al. 1996). The parent sample for this project has the original criterion of $f_\nu(60\mu\text{m}) \gtrsim 3$ Jy, a published redshift, and no active galactic nucleus or Seyfert classification in the NED, although two galaxies of the sample, NGC4418 and MRK331, show some evidences of hosting an AGN. They span the full range of morphologies, mostly spirals and irregular galaxies, but including two elliptical galaxies; FIR luminosities are $\sim 10^8$ - 10^{12} L_\odot ; FIR colors are $f_\nu(60\mu\text{m})/f_\nu(100\mu\text{m}) \sim 0.25 - 1.6$, and infrared to blue luminosity ratios $L_{\text{FIR}}/L_B \sim 0.05 - 50$. They observed 61 galaxies with the broadband filters, LW2 ($6.75 \mu\text{m}$, $\delta\lambda = 3.5 \mu\text{m}$) and LW3 ($15.0 \mu\text{m}$, $\delta\lambda = 6.0 \mu\text{m}$) of ISOCAM (Cesarsky et al. 1996). For this work, we did not include 7 galaxies (NGC1222, UGC2855, NGC2366, NGC4490, NGC5866, NGC6822, and NGC6946), that either have only lower limits in their MIR observations, or are not detected in any LW filter.

For the majority of the galaxies we have also collected, from literature, total fluxes on radio emission at 6.3 and 21 cm (Condon et al. 1990, 1991, 1995), that will be used for the characterization of the starburst evolution. All these data are shown in Table 4.

Fig. 3 shows the location of the galaxies in the regions corresponding to different star formation activities, following the definition by Lu et al. (2003). About 43% galaxies of the sample have $\log(L_{\text{FIR}}/L_B) \geq 0$ and $\log f_\nu(60\mu\text{m})/f_\nu(100\mu\text{m}) \geq -0.24$, and are considered to be strong starbursts. About 31% galaxies of the sample fall in the opposite quadrant and are considered to be FIR-quiet galaxies, while the remaining 26%, populating the other two quadrants, are considered to be in a mild starburst phase. In summary the sample of Dale et al. is well suited to study a mild to strong starburst environment.

4.2 Results of the comparison

In the four panels of Fig. 4 we plot the observed ISO LW2 and LW3 and IRAS 12, 25, 60 and $100 \mu\text{m}$ flux ratios. The

LW2 filter includes the 6.2, 7.7, and $8.6\mu\text{m}$ PAH bands while the LW3 filter includes the 11.9, 12.7 and 16.4 bands, but it is less affected by PAHs as compared to the LW2. Finally also the IRAS $12\mu\text{m}$ band is dominated by the emission of the 11.3, 11.9 and 12.7 PAHs.

Nearby star forming galaxies are known to follow a well-defined trend in the IRAS flux density ratios $f_\nu(12\mu\text{m})/f_\nu(25\mu\text{m})$ versus $f_\nu(60\mu\text{m})/f_\nu(100\mu\text{m})$ (Helou 1986; Dale et al. 2001). This trend is in the sense that at increasing $f_\nu(60\mu\text{m})/f_\nu(100\mu\text{m})$ the $f_\nu(12\mu\text{m})/f_\nu(25\mu\text{m})$ and $f_\nu(6.75\mu\text{m})/f_\nu(15\mu\text{m})$ ratios decrease. This has been explained as an increasing sequence of star formation activity. The warmer $f_\nu(60\mu\text{m})/f_\nu(100\mu\text{m})$ color reflects the fact that higher dust temperatures of big grains (in thermal equilibrium) shift the FIR emission peak to shorter wavelengths. The common interpretation of the $f_\nu(12\mu\text{m})/f_\nu(25\mu\text{m})$, $f_\nu(6.75\mu\text{m})/f_\nu(15\mu\text{m})$ behavior is that, at the same time, the stronger radiation field destroys very small grains and PAHs (see Section 2.2) and enhances the MIR continuum as well.

In that figure, we have superimposed the time evolution of models computed with three different values of the MCs optical depth, $\tau_1 = 40, 50$ and 60 , and two escape timescales of newly born stars from their parent MCs, $t_{\text{esc}} = 10$ Myr and $t_{\text{esc}} = 30$ Myr. The time evolution is indicated by the ratio between the age of the starburst and the e-folding time of the star formation process (age_b/t_b), from the beginning of the starburst phase ($age_b/t_b \sim 0.05$) to the quiescent phase ($age_b/t_b \sim 4.0 - 7.92$). The ticks correspond to different values of the ratio $age_b/t_b = 0.05, 0.08, 0.12, 0.20, 0.31, 0.50, 0.80, 1.26, 2.00, 3.15, 5.0$, and 7.92 , and the evolution is defined by the lines. The SEDs of our models are initially dominated by emission of the underlying quiescent disk component which is characterized by cold FIR colors ($\text{Log}(f_\nu(60\mu\text{m})/f_\nu(100\mu\text{m})) \leq -0.3$). As their luminosity increases, due to the rapid formation of new massive stars, they evolve toward hotter FIR colors, reaching a maximum when the starburst is well developed ($\text{Log}(f_\nu(60\mu\text{m})/f_\nu(100\mu\text{m})) \geq 0$). Then they turn back toward cooler FIR colors (but with higher $f_\nu(12\mu\text{m})/f_\nu(25\mu\text{m})$ and $f_\nu(6.75\mu\text{m})/f_\nu(15\mu\text{m})$ colors) as the star formation declines and the oldest stars leave the molecular clouds. This behavior is common to all the selected starburst models.

The agreement with the data is fairly good. In addition we may draw the following considerations.

We did not include a PAH destruction mechanism continuously increasing with the intensity of the radiation field, instead we made the assumption that within star forming regions PAHs are damped by a fixed factor (see Sec. 2.2). Therefore the lowering of the $f_\nu(6.75\mu\text{m})/f_\nu(25\mu\text{m})$ and $f_\nu(6.75\mu\text{m})/f_\nu(15\mu\text{m})$ colors in the models simply reflects the progressive dominance of the MC component over the cirrus one, when the starburst is in its star formation peak. The sequence of colors is then interpreted as an evolutionary sequence characterized by the dominance of the MC over the cirrus component (Helou 1986; Helou et al. 1991). Four main evolutionary phases can be recognized: the early starburst phase characterized by cool $f_\nu(60\mu\text{m})/f_\nu(100\mu\text{m})$ colors and low MIR-FIR colors; the peak starburst phase with the models reaching the hottest FIR colors and the lowest MIR-FIR colors; the evolved starburst phase with warm FIR colors

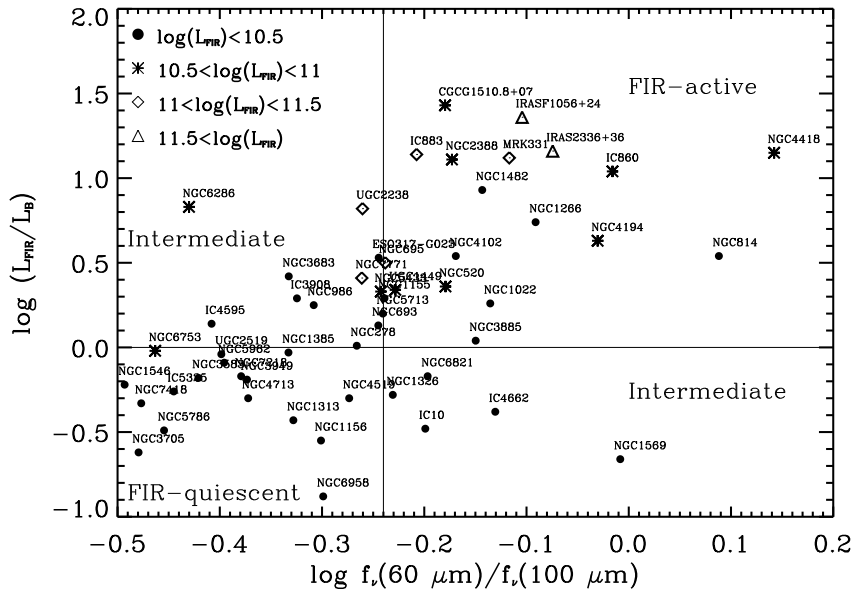


Figure 3. $\log(L_{\text{FIR}}/L_{\text{B}})$ versus $\log f_{\nu}(60\mu\text{m})/f_{\nu}(100\mu\text{m})$ for the galaxies of the Dale et al. (2000) sample. Different symbols indicate different FIR luminosities.

and warm MIR-FIR colors; finally the post starburst phase where the models move toward the cool FIR colors and hot MIR-FIR colors, typical of normal spiral galaxies.

The models considered here do not reach the coolest FIR region of the diagram ($f_{\nu}(60\mu\text{m})/f_{\nu}(100\mu\text{m}) \leq -0.45$). This is the region dominated by normal spiral galaxies as can be seen by the location of the Boselli et al. (2003) Virgo spiral galaxy sample, plotted for the purpose of comparison (open circles). In this paper we have considered models meant to reproduce actively star forming galaxies. It is conceivable that the coolest region requires a more direct consideration of the PDRs (see Section 2.2).

The evolution of the starbursts in the diagrams is modulated by the optical depth of the molecular clouds, which affects primarily the colors $f_{\nu}(6.75\mu\text{m})/f_{\nu}(60\mu\text{m})$ and $f_{\nu}(15\mu\text{m})/f_{\nu}(60\mu\text{m})$. At larger optical depths these flux ratios decrease. The flux ratio $f_{\nu}(6.75\mu\text{m})/f_{\nu}(15\mu\text{m})$ is instead less dependent on τ_1 , and in this case both data and models show a lower dispersion. Furthermore the range of allowed optical depths is fairly narrow, ranging from $\tau_1 \sim 40$ to ~ 60 . Only a few objects would require a slightly higher optical depth. These objects are particular in the sense that they do not share the trend common to all the others and the majority of them are actually ULIRGs, which could be highly obscured (Prouton et al. 2004).

The effect of other tested parameters are in brief the following: shorter e-folding times t_b of the burst produce hotter peak models. However these models are also characterized by a wider evolutionary sequence in the MIR colors; in practice with $t_b \lesssim 15$ Myr, the evolutionary path is an envelope of the data without matching them. For values of $t_b \gtrsim 25$ Myr, the evolution of the MIR colors is as observed but the range of the 60/100 color is very small and concentrated to the warm central region. The escape timescale of young stars from their parent MCs is well constrained by this

comparison. Short escape times, $t_{\text{esc}} \lesssim 10$ Myr, result in too wide evolutionary sequences, in the MIR-FIR plots, again surrounding the data, while values higher than $t_{\text{esc}} \sim 35$ Myr are confined to low MIR-FIR flux ratios. The typical escape time suggested by the data is of ~ 20 Myr, comparable to the e-folding time of the SFR. As for the molecular gas fraction, the comparison suggests that it should be confined between 30% and 70% of the total gas mass, with 50% the best value.

Summarizing, from the comparison with the data we find the following typical parameters for our models: a star formation e-folding time $t_b \sim 15 - 25$ Myr; fractions of molecular mass between 0.3 to 0.7, with the hottest models having the lowest molecular gas fraction; escape times t_{esc} between 10 to 40 Myr.

4.3 ISO-IRAS-Radio color-color plots

For the majority of the galaxies radio data at 6.2 and 21cm are available (see Table 4). The radio emission of the models is computed following the prescriptions given in Bressan, Silva & Granato (2002). Thermal emission is computed according to the flux of ionizing photons, while the non thermal emission is set proportional to the core collapse supernova rate.

The FIR to radio ratio q is defined as:

$$q = \log \frac{F_{\text{FIR}}/(3.75 \times 10^{12} \text{Hz})}{f_{\nu}(1.49 \text{GHz})/(\text{W m}^{-2} \text{Hz}^{-1})} \simeq 2.35 \pm 0.2 \quad (1)$$

where $F_{\text{FIR}} = 1.26 \cdot 10^{-14} (2.58 f_{\nu}(60\mu\text{m}) + f_{\nu}(100\mu\text{m})) \text{ W m}^{-2}$, with $f_{\nu}(60\mu\text{m})$ and $f_{\nu}(100\mu\text{m})$ in Jy. The average observed value of the q parameter for a spiral galaxy is $q \simeq 2.35$ at 1.49 GHz (Condon 1992; Sanders & Mirabel 1996)

Fig. 5 shows the evolution of the models in composite MIR-FIR-radio bands. The agreement between models and

Table 4. Properties of the Dale et al. (2000) sample we use for our analysis. Radio data are from Condon et al. (1990, 1991, 1995).

	NAME	12 μ m	25 μ m	60 μ m	100 μ m	6.75 μ m	15 μ m	D_L	$\log(\frac{L_{FIR}}{L_B})$	6.3 cm	21 cm
		IRAS Jy	IRAS Jy	IRAS Jy	IRAS Jy	ISO-LW2 Jy	ISO-LW3 Jy			Mpc	Jy
1	IC10	4.88	13.95	112.92	178.56	2.18	3.06	0.7	-0.48	0.202	0.298
2	NGC278	1.63	2.57	25.05	46.22	1.12	1.18	11.8	0.01	0.063	0.138
3	NGC520	0.76	2.84	31.10	46.99	0.52	0.86	31.6	0.36	0.126	0.177
4	NGC693	0.29	0.55	6.73	11.83	0.18	0.18	22.1	0.13	0.033	0.053
5	NGC695	0.48	0.86	7.87	13.62	0.25	0.36	131.8	0.50	0.025	0.076
6	UGC1449	0.31	0.56	4.96	8.39	0.18	0.17	75.5	0.34	-	-
7	NGC814	0.19	1.01	4.41	3.60	0.05	0.22	21.4	0.54	-	0.007
8	NGC986	1.41	3.65	25.14	51.11	0.51	1.07	25.2	0.25	0.040	0.110
9	NGC1022	0.75	3.29	19.83	27.09	0.31	0.77	19.4	0.26	0.018	0.045
10	UGC2238	0.34	0.53	8.40	15.30	0.24	0.30	86.8	0.82	0.040	0.217
11	NGC1155	0.21	0.47	2.89	5.01	0.05	0.09	60.3	0.29	0.018	-
12	NGC1156	0.17	0.55	5.24	10.48	0.09	0.14	6.4	-0.55	-	0.022
13	NGC1222	0.51	2.29	13.07	15.45	0.27	-	32.6	0.44	0.029	0.055
14	UGC2519	0.25	0.34	2.98	7.46	0.12	0.17	34.6	-0.04	-	-
15	NGC1266	0.14	1.23	13.32	16.43	0.04	0.15	29.1	0.74	-	0.110
16	NGC1313	1.70	3.75	45.69	97.25	0.69	0.84	3.7	-0.43	0.123	-
17	NGC1326	0.38	0.86	8.17	13.90	0.18	0.32	16.2	-0.28	0.035	0.031
18	NGC1385	1.19	2.02	17.30	37.23	0.72	0.76	18.4	-0.03	0.078	0.162
19	UGC2855	2.93	4.86	42.39	90.49	-	-	18.7	0.31	0.135	-
20	NGC1482	1.54	4.67	33.45	46.53	0.78	1.37	24.0	0.93	0.125	0.216
21	NGC1546	0.62	0.79	7.21	22.44	0.42	0.56	14.1	-0.22	-	-
22	NGC1569	1.23	8.98	54.25	55.30	0.32	1.43	2.5	-0.66	0.202	0.411
23	NGC2388	0.51	2.07	17.01	25.33	0.23	0.50	54.8	1.11	0.027	0.073
24	NGC2366	0.21	1.05	4.85	5.04	0.02	0.17	2.9	-0.83	-	0.025
25	ESO317-G023	0.34	0.88	13.50	23.71	0.18	0.27	34.7	0.53	-	0.075
26	IRASF1056+24	0.17	1.19	12.08	15.36	0.09	0.27	171.4	1.36	0.020	0.050
27	NGC3583	0.63	0.78	7.08	18.66	0.29	0.41	29.2	-0.18	0.030	0.053
28	NGC3620	1.29	4.71	46.80	67.26	0.63	1.06	19.0	5.00	0.120	-
29	NGC3683	1.06	1.53	13.61	29.27	0.64	0.76	24.2	0.42	0.045	0.099
30	NGC3705	0.38	0.44	3.72	11.22	0.19	0.27	11.9	-0.62	-	0.021
31	NGC3885	0.46	1.41	11.66	16.46	0.33	0.45	20.8	0.04	-	0.046
32	NGC3949	0.82	1.37	11.28	26.65	0.42	0.50	11.6	-0.19	0.037	0.100
33	NGC4102	1.72	7.05	48.10	71.01	0.66	1.61	12.4	0.54	0.070	0.261
34	NGC4194	0.83	4.53	23.72	25.44	0.41	0.84	34.8	0.63	0.039	0.102
35	NGC4418	1.00	9.69	43.89	31.64	0.24	1.56	27.3	1.15	-	0.039
36	NGC4490	1.86	4.20	45.90	76.93	-	-	8.2	-0.20	0.295	0.779
37	NGC4519	0.36	0.55	3.74	7.02	0.11	0.23	15.1	-0.30	0.006	0.009
38	NGC4713	0.24	0.17	4.60	10.84	0.15	0.21	7.4	-0.30	-	0.038
39	IC3908	0.44	0.87	8.09	17.08	0.44	0.43	15.4	0.29	0.440	0.079
40	IC860	0.10	1.31	17.93	18.60	0.02	0.06	44.7	1.04	4.000	0.033
41	IC883	0.25	1.36	15.44	24.90	0.16	0.25	94.0	1.14	0.046	0.101
42	NGC5433	0.27	0.70	6.62	11.57	0.18	0.30	59.0	0.33	-	0.059
43	NGC5713	1.30	2.84	21.89	38.09	0.88	1.06	24.7	0.20	0.081	0.154
44	NGC5786	0.36	0.76	5.26	14.98	0.30	0.39	37.9	-0.49	-	0.040
45	NGC5866	0.36	0.34	5.21	17.11	-	-	11.4	-0.61	-	0.021
46	CGCG1510.8+07	0.05	0.83	20.84	31.52	0.04	0.08	52.4	1.43	-	-
47	NGC5962	0.74	1.03	8.89	22.11	0.37	0.51	27.3	-0.09	0.036	0.077
48	IC4595	0.71	0.73	7.05	18.04	0.30	0.39	42.9	0.14	0.035	0.062
49	NGC6286	0.42	0.56	8.22	22.13	0.17	0.20	76.5	0.83	0.050	0.156
50	IC4662	0.30	1.27	8.81	11.90	0.05	0.17	2.1	-0.38	0.029	-
51	NGC6753	0.60	0.72	9.43	27.40	0.38	0.51	40.4	-0.02	0.035	-
52	NGC6821	0.14	0.31	3.63	5.71	0.06	0.13	22.5	-0.17	-	-
53	NGC6822	0.84	6.63	58.86	130.32	0.10	0.31	0.7	-0.58	-	0.048
54	NGC6946	15.17	23.34	167.72	362.66	11.19	11.49	5.5	-0.34	0.493	1.395
55	NGC6958	0.16	0.20	1.00	1.99	0.03	0.03	36.4	-0.88	-	0.018
56	NGC7218	0.28	0.56	4.67	11.18	0.21	0.28	23.8	-0.17	-	-
57	NGC7418	0.63	0.69	5.38	16.13	0.23	0.29	19.4	-0.33	-	0.046
58	IC5325	0.48	0.70	5.15	14.35	0.24	0.31	19.7	-0.26	-	-
59	IRAS2336+36	0.13	0.88	7.44	8.83	0.02	0.11	261.2	1.16	-	-
60	NGC7771	0.87	2.18	20.50	37.40	0.46	0.59	60.0	0.41	0.060	0.124
61	MRK331	0.55	2.39	18.04	23.61	0.21	0.52	76.8	1.12	0.028	0.068

data is fairly good, consistent with the fact that the models well reproduce the observed FIR-radio correlation. The partial disagreements in the 21 cm plots for models during the peak phase may be explained by the need to account for free-free absorption (Bressan et al. 2002; Prouton et al. 2004). Again, the region of very quiescent spiral galaxies is not covered by the starburst models.

5 CONCLUSIONS

This paper is devoted to an accurate analysis of the properties of starburst galaxies in the mid infrared. This spectral region is dominated by PAH emission features, and an update with respect to our previous treatment of PAHs in our code GRASIL (Silva et al. 1998) was necessary in its two main components, the cirrus and the molecular clouds, respectively.

In the cirrus component we have introduced the new

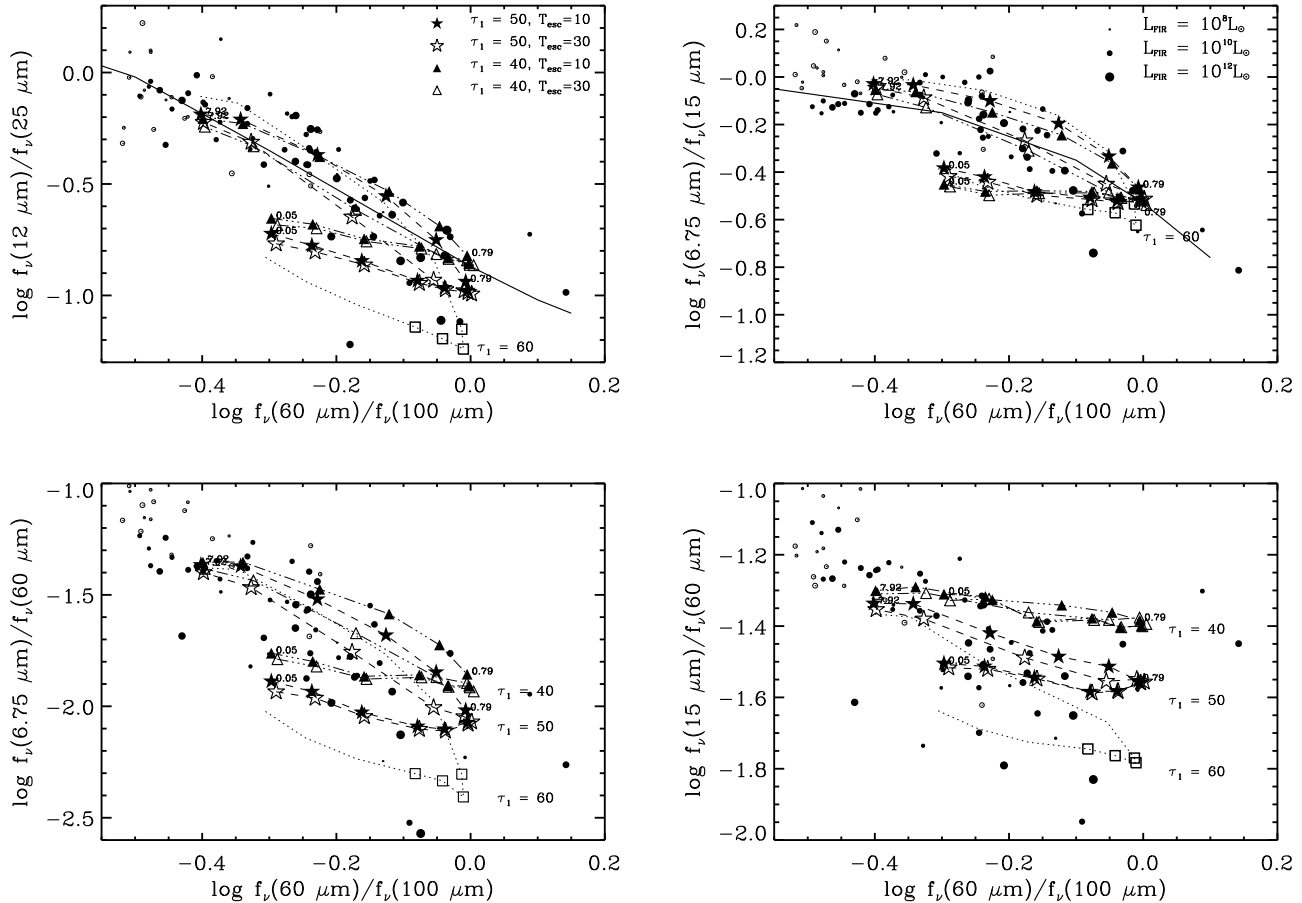


Figure 4. IRAS-ISO color-color diagrams for the Dale et al. sample. Black circles are the data. Different symbols are different optical depths of MCs ($\tau_{1\mu m}$) and escape times of newly born stars from MCs (t_{esc}). The parameters of the models are $t_b = 20$ Myr, fraction of molecular gas mass to total gas mass=0.5. The ticks correspond to $\frac{age_b}{t_b} = 0.05, 0.08, 0.12, 0.20, 0.31, 0.50, 0.80, 1.26, 2.00, 3.15, 5.0,$ and 7.92. The lines connect the different evolution sequences. In order to remark the region occupied by the normal spiral galaxies, we also plot the Boselli et al. (2003) sample as open circles (see text for details). The sizes of the symbols represent the FIR luminosities as marked by the legend in the top right panel.

quantitative description of PAHs in the diffuse ISM, given by Li & Draine (2001). As for the MC component, the observational evidence of a lack of PAH emission in regions characterized by strong UV radiation fields, forced us to reduce the PAHs abundance by a large factor (i.e. ~ 1000 times less than in the cirrus component).

As a workbench we have compared the updated model with the SEDs of a select sample of star forming galaxies, for which both accurate MIR narrow band and NIR, FIR and Radio observations are available. This comparison probes successfully over the wide range of FIR luminosities of the selected galaxies.

We have then analyzed the observed trend of MIR-FIR and radio colors for a larger sample of galaxies, from actively star forming to obscured starbursts. To this aim we have compared a large library of model SEDs, spanning a wide range of physical parameters, with observed color-color plots. The data are well reproduced by the models within a limited range of values of the main physical parameters.

As already suggested by Helou (1986) and Dale et al (2001), the observed MIR-FIR trend can be interpreted as

a sequence of the dominance of the MC component with respect to the cirrus component. However, contrary to previous works, that were based on mainly empirical SEDs, this comparison allows us to propose that the observed sequence corresponds to the evolution of the starburst phenomenon.

Four main phases can be highlighted, as summarized in Fig. 6:

(a) The early starburst phase, characterized by warm FIR and cold MIR colors and where the few newly formed stars are still deep inside the progenitor molecular clouds. The SED is dominated by emission from MCs but the intensity of the radiation field has not reached its peak value. In our model this phase has a low ratio of age_b/t_b , between 0.05 to 0.20.

(b) The starburst peak phase, where the majority of massive stars are produced, and the SED is dominated by the hot dust emission from the molecular cloud component. During this phase the starburst reaches the hottest FIR colors and the lowest relative PAH emission. It is characterized by

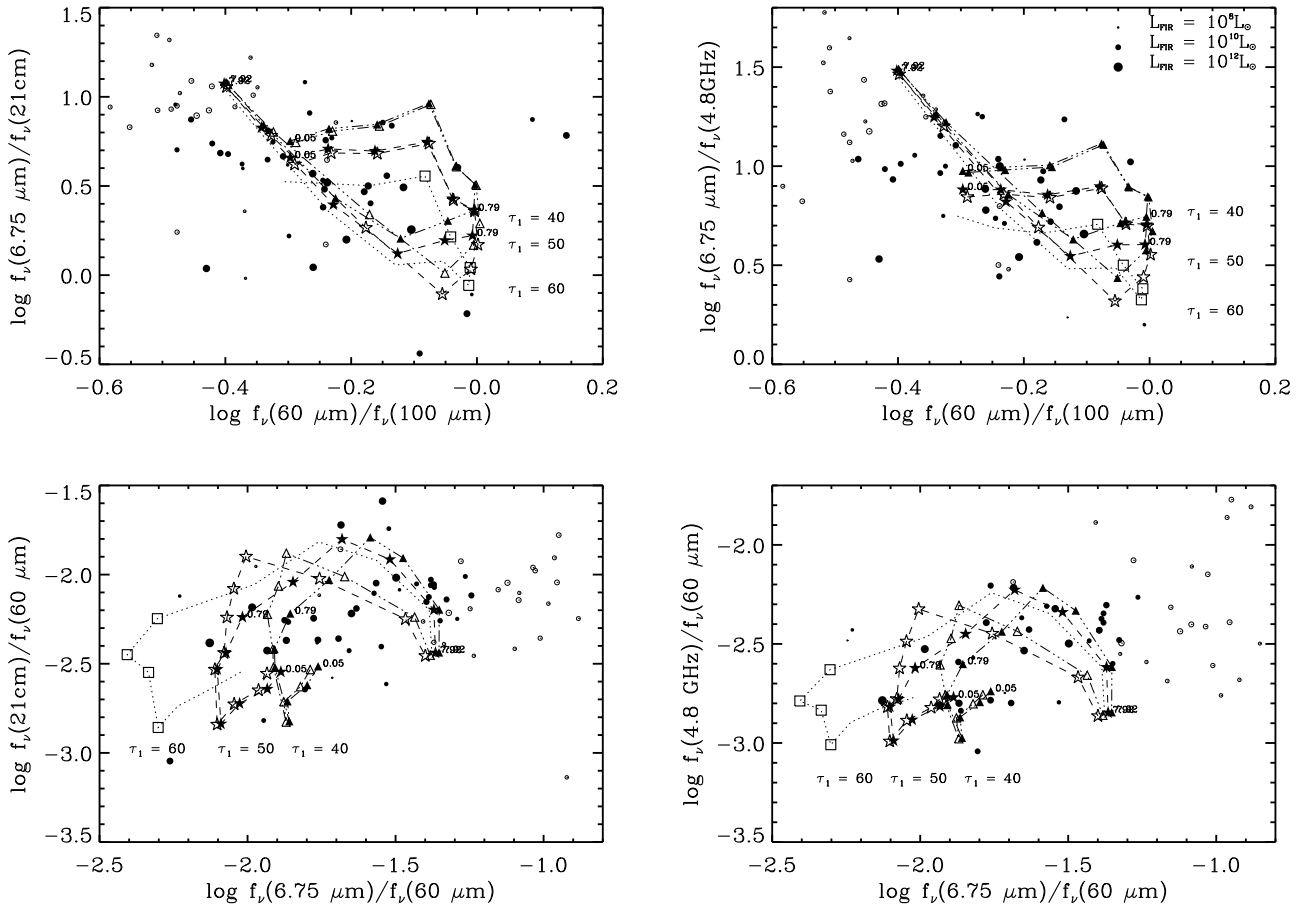


Figure 5. IRAS-ISO-radio color-color diagrams for the Dale et al. sample. Black circles are the data. Different symbols are different optical depths τ_1 and escape timescales t_{esc} . The parameters of the models are: $t_b = 20$ Myr, fraction of molecular mass = 0.5. The ticks correspond to $\frac{age_b}{t_b} = 0.05, 0.08, 0.12, 0.20, 0.31, 0.50, 0.80, 1.26, 2.00, 3.15, 5.0, \text{ and } 7.92$. The lines connect the different evolutionary sequences. In order to remark the region occupied by the normal spiral galaxies, we plot the Boselli et al. (2003) spiral galaxy sample as open circles. The sizes of the symbols represents the FIR luminosities.

age_b/t_b between 0.30 to 2.0, and the young stars are still mostly embedded in the parent molecular clouds.

(c) The evolved starburst phase, where the number of newly formed stars has drastically decreased and, at the same time, most of the still hot stars are out of the progenitor MCs and heat the cirrus. The emission in this phase, which lasts between $age_b/t_b \simeq 2.0$ to 4.0, is dominated by the cirrus component.

(d) The post-starburst phase, $age_b/t_b > 4$, where the current SFR is mainly due to the quiescent disk and all the stars formed during the starburst are now outside the MC. The FIR and MIR colors are evolving toward those of normal spiral galaxies.

The data suggest that the starburst phenomenon is characterized by a surprising homogeneity. The optical depth of the molecular clouds at $1 \mu\text{m}$ is confined between 40 and 60; the escape time scale from molecular clouds is between 10 and 30 Myr and it mainly affects the advanced evolution of the starburst; the e-folding time of the star formation process cannot be shorter than about 15 Myr, nor larger than about 30 Myr. Though those figures are similar

to the estimates given in Silva et al. (1998), only with the advent of accurate measurements in the mid infrared it has been possible to restrict them to a very narrow range.

It is also evident from the models, that PAH features cannot be taken as a direct measure of the dominant powering mechanism since, in those cases where the MC component dominates, there is a significant lack of emission, as observed in AGNs.

Further work is needed to reproduce the most quiescent galaxies (occupying the region with the coldest FIR colors, $\text{Log}(f_\nu(60\mu\text{m})/f_\nu(100\mu\text{m})) \leq -0.45$), where possibly a more complex description and modelling of the different zones of star formation, for instance the PDR zones, is required, and will be the subject of a forthcoming paper.

ACKNOWLEDGEMENTS

We would like to thank the anonymous referee whose comments have helped to improve the paper. O. Vega and M. Chavez acknowledge the support of INAOE and the Mexican CONACYT project 36547 E; O. Vega also acknowledges

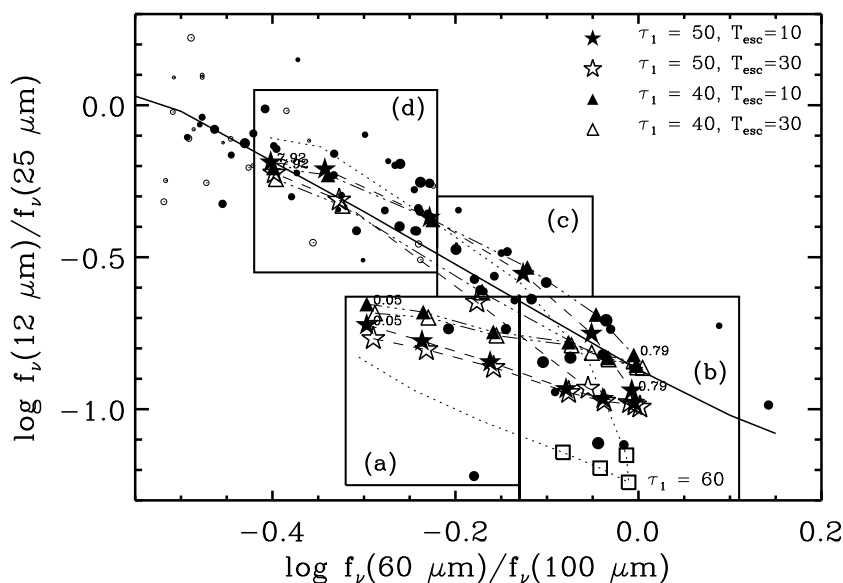


Figure 6. IRAS color-color diagrams for the Dale et al. sample. Meaning of symbols is as in Fig. 4. The four closed regions highlight the four main evolutionary phases of our starburst models with which we interpret the behavior of data. See text for more details.

the support of the Mexican CONACYT project 39714 F; L. Silva, A. Bressan and G. L. Granato acknowledge warm hospitality by INAOE.

REFERENCES

- Abergel A., Boulanger F., Mizuno A., Fukui Y., 1994, *ApJ*, 423, 59
- Allain T., Leach S., Sedlmayr E., 1996, *A&A*, 305, 616
- Allamandola L. J., Tielens A. G. G. M., Barker J. R., 1985, *ApJ*, 290, 25
- Armus, L. et al., 2004, *ApJS*, 154, 178
- Beintema D. A., van den Ancker M. E., Molster F. J., Waters L. B. F. M., Tielens A. G. G. M., Waelkens C., de Jong T., de Graauw T., Justtanont K., Yamamura I., Heras A., Lahuis F., Salama A., 1996, *A&A*, 315, 369
- Bendo et al., 2002, *AJ*, 123, 3067
- Boselli A., Sauvage M., Lequeux J., Donati A., Gavazzi G., 2003, *A&A*, 406, 867
- Boselli A., Lequeux J., Gavazzi G., 2004, *A&A*, 428, 409
- Boulanger F. et al., 1996, *A&A*, 315, 325
- Boulanger F., 2000, *ISO Beyond Point Sources: Studies of Extended Infrared Emission*, ESA-SP 455, p. 3
- Bressan A., Silva L., Granato G. L., 2002, *A&A*, 392, 377
- Carico D. P., Keene J., Soifer B. T., Neugebauer G., 1992, *PASP*, 104, 1086
- Cesarsky C. J., et al., 1996, *A&A*, 315, 32
- Chini R., Kruegel E., Lemke R., Ward-Thompson D., 1995, *A&A*, 295, 317
- Chini R., Kruegel E., Lemke R., 1996, *A&AS*, 118, 47
- Clavel J., Schulz B., Altieri B., Barr P., Claes P., Heras A., Leech K., Metcalfe L., Salama, A., 2000, *A&A*, 357, 839
- Condon J. J., Helou G., Sanders D. B., & Soifer B. T., 1990, *ApJS*, 73, 359
- Condon J. J., Frayer D. T., Broderick, J. J., 1991, *AJ*, 101, 362
- Condon J. J., 1992, *ARA&A*, 30, 575
- Condon J. J., Frayer D. T., Broderick J. J., 1995, *ADIL*, JC, 02
- Contursi A., Lequeux J., Cesarsky D., Boulanger F., Rubio M., Hanus M., Sauvage M., Tran D., Bosma A., Madden S., Vigroux L., 2000, *A&A*, 362, 310
- Dale D. et al., 2000, *ApJ*, 120, 583
- Dale D., Helou G., Contursi A., Silbermann N. A., Kolhatkar S., 2001, *ApJ*, 459, 215
- Dale D. et al., 2005, *astro-ph/0507645*
- Dopita M. A., Groves B. A., Fischera J., Sutherland R. S., Tuffs R. J., Popescu C. C., Kewley L. J., Reuland M., Leitherer C., 2005, *ApJ*, 619, 755
- Draine B. T., Lee H. M., 1984, *ApJ*, 285, 89
- Draine B. T., 2003, *ARA&A*, 41, 241
- Dunne L., Eales S., Edmunds M., Ivison R., Alexander P., Clements D. L., 2000, *MNRAS*, 315, 115
- Dwek E., 2004, *ApJ*, 611, L109
- Engelbracht C. W., Gordon K. D., Rieke G. H., Werner M. W., Dale D. A., Latter W. B., 2005, *ApJ*, 628, 29
- Forster Schreiber N. M., Sauvage M., Charmandaris V., Laurent O., Gallais P., Mirabel I. F., Vigroux L., 2003, *A&A*, 399, 833
- Forster Schreiber, N. M., Roussel H., Sauvage M., Charmandaris V., 2004, *A&A*, 419, 501
- Galliano F., Madden S. C., Jones A. P., Wilson C. D., Bernard, J.-P., Le Peintre F., 2003, *A&A*, 407, 159
- Galliano F., Madden S. C., Jones A. P., Wilson C. D., Bernard, J.-P., 2005, *A&A*, 434, 867
- Genzel R. et al., 1998, *ApJ*, 498, 579
- Granato G. L., Lacey C. G., Silva L., Bressan A., Baugh C. M., Cole S., Frenk C. S., 2000, *ApJ*, 542, 710
- Helou G., 1986, *ApJ*, 311, L33
- Helou G., Ryter C., Soifer B. T., 1991, *ApJ*, 376, 505
- Helou G. et al., 1996, *AAS*, 189, 6704
- Helou G., Lu N. Y., Werner M. W., Malhotra S., Silbermann N., 2000, *ApJ*, 532, 21
- Hony S., Van Kerckhoven C., Peeters E., Tielens A. G. G. M., Hudgins D. M., Allamandola L. J., 2001, *A&A*, 370, 1030
- Israel F. P., van der Hulst J. M., 1983, *AJ*, 88, 1736
- Laor A., Draine B. T., 1993, *ApJ*, 402, 441
- Laurent O., Mirabel I. F., Charmandaris V., Gallais P., Madden S. C., Sauvage M., Vigroux L., Cesarsky C., 2000, *A&A*, 359, 887

- Leger A., Puget J. L., 1984, *A&A*, 137, 5
- Leger A., D'Hendecourt L., Defourneau D., 1989, *A&A*, 216, 148
- Li A., Draine B. T., 2001, *ApJ*, 554, 778
- Lu N., Helou G., Werner M. W., Dinerstein H. L., Dale D. A., Silbermann N. A., Malhorta S., Beichman C. A., Jarret T. H., 2003, *ApJ*, 588, 199
- Lutz D., Genzel R., Kunze D., Spoon H. W. W., Sturm E., Sternberg A., Moorwood A. F. M., 1998, *ASPC*, 132, 89
- Machalski J., Condon J. J., 1999, *ApJS*, 123, 41
- Madden S., 2000, *NewAR*, 44, 249
- Madden S., 2005, *AIPC*, 761, 223
- Marty P., Serra G., Chaudret B., Ristorcelli I., 1994, *A&A*, 282, 916
- Mattila K., Lemke D., Haikala L. K., Laureijs R. J., Leger A., Lehtinen K., Leinert C., Mezger P. G., 1996, *A&A*, 315, 353
- Metcalfe L., Steel S. J., Barr P., Clavel J., Delaney M., Gallais P., Laureijs R. J., Leech K., McBreen B., Ott S., Smith N., Hanlon L., 1996, *A&A*, 315, 105
- Moutou C., Leger A., D'Hendecourt L., 1996, *A&A*, 310, 297
- Niklas S., Klein U., Braine J., Wielebinski R., 1995, *A&AS*, 114, 21
- Panuzzo P., Bressan A., Granato G. L., Silva L., Danese L., 2003, 409, 99
- Panuzzo P., Silva L., Granato G. L., Bressan A., Vega O., 2005, in Popescu C. C., Tuffs R. J., eds, *AIP Conference Proceedings* 761, p. 187
- Peeters E., Spoon H. W. W., Tielens A. G. G. M., 2004a, *ApJ*, 613, 986
- Peeters E., Allamandola L. J., Hudgins D. M., Hony S., Tielens A. G. G. M., 2004b, in Witt N. A., Clayton G. C., Draine B. T., eds, *ASP Conference Series*, Vol. 309, p.141
- Peeters E., Mattioda A. L., Hudgins D. M., Allamandola L. J., 2004c, *ApJ*, 617, 65
- Prouton O. R., Bressan A., Clemens M., Franceschini A., Granato G. L., Silva L., 2004, *A&A*, 421, 115
- Puget J. L., Leger A., 1989, *ARA&A*, 27, 161
- Rigopoulou D., Spoon H. W. W., Genzel R., Lutz D., Moorwood A. F. M., Tran Q. D., 1999, *AJ*, 118, 2625
- Roussel H., Sauvage M., Vigroux L., Bosma A., 2001, *A&A*, 372, 427
- Salpeter E. E., 1955, *ApJ*, 121, 161
- Sanders D. B., Mirabel I. F., 1996, *ARA&A*, 34, 749
- Serra G., Chaudret B., Saillard Y., Le Beuze A., Rabaa H., Ristorcelli I., Klotz A., 1992, *A&A*, 260, 489
- Silva L., Granato G. L., Bressan A., Danese L., 1998, *ApJ*, 509, 103
- Silva L., 1999, PhD Thesis, SISSA, Trieste, Italy
- Smith J. D. T. et al., 2004, *ApJS*, 154, 199
- Tacconi-Garman L. E., Sturm E., Lehnert M., Lutz D., Davies R. I., Moorwood A. F. M., 2005, *A&A*, 432, 91
- Tielens A. G. G. M., Hony S., van Kerckhoven C., Peeters E., 1999, in *The Universe as Seen by ISO*. Eds. P. Cox M. F. Kessler. *ESA-SP 427.*, p. 579
- Tielens A. G. G. M., 1999, *Formation and Evolution of Solids in Space*, Edited by J. Mayo Greenberg Aigen Li. Kluwer Academic Publishers, p.33
- Verstraete L., Puget J. L., Falgarone E., Drapatz S., Wright C. M., Timmermann, R., 1996, *A&A*, 315, 337
- Vigroux L., Mirabel F., Altieri B., Boulanger F., Cesarsky C., Cesarsky D., Claret A., Fransson C., Gallais P., Levine D., Madden S., Okumura K., Tran D., 1996, *A&A*, 315, 93
- Weedman D. W., Hao L., Higdon S. J. U., Devost D., Wu Y., Charmandaris V., Brandl B., Bass E., Houck J. R., 2005, *astro-ph/0507423*
- Xu C., de Zotti G., 1989, *A&A*, 225, 12
- Zubko V., Dwek E., Arendt R. G., 2004, *ApJS*, 152, 211